International Journal of Thermophysics, Vol. 27, No. 2, March 2006 (© 2006)
DOI: 10.1007/s10765-005-0008-z

A Novel Instrument for the Measurement of the Thermal Conductivity of Molten Metals. Part I: Instrument's Description

M. V. Peralta-Martinez,[1] M. J. Assael,[2,3] M. J. Dix,[4] L. Karagiannidis,[5] and W. A. Wakeham[6]

Received April 27, 2005

The paper reports the design and construction of a new instrument for the measurement of the thermal conductivity of molten metals and salts. The apparatus is based on the transient hot-wire technique, and it is intended for operation over a wide range of temperatures, from ambient up to 1200 K. The present experimental technique overcomes problems of convection and thermal radiation, and it is demonstrated that it operates in accord with a theoretical model. The uncertainty of the thermal conductivity results is estimated to be ±2% which is superior to that achieved in most earlier work.

KEY WORDS: molten metals; thermal conductivity; transient hot wire.

1. INTRODUCTION

The thermal conductivity of molten metals is an important thermophysical property with technological importance in several fields such as metallurgy,

[1] Instituto de Investigaciones Eléctricas, Gerencia de Procesos Térmicos, Palmira, 62490 Cuernavaca Morelos, México.
[2] Department of Chemical Engineering, Aristotle University of Thessaloniki, Thessaloniki 54124, Greece.
[3] To whom correspondence should be addressed. E-mail: assael@auth.gr
[4] Department of Chemical Engineering and Chemical Technology, Imperial College London, London SW7 2AZ, United Kingdom.
[5] FARMACHEM SA, Manufacturers and Traders of Agrochemicals, P.O. Box 26, Sindos 570 22, Thessaloniki, Greece.
[6] School of Engineering Sciences, University of Southampton, Highfield, Southampton SO17 1BJ, United Kingdom.

ceramic engineering, and glass manufacture, among others. Molten metals also have applications as heat transfer fluids, for heat storage, and in high temperature thermometers. However, despite the fact that all these industries and processes require accurate data, several reviews of the thermal conductivity of molten metals [1–4] have revealed discrepancies as large as 50% among the experimental data reported in the literature by various authors over a wide range of temperature. The lack of accurate data is attributed to the inaccuracy of the experimental techniques where the main problem is the phenomenon of natural convection, which becomes much more difficult to avoid at high temperatures, since temperature control and distribution becomes more difficult as the temperature increases.

The new experimental technique developed here overcomes the problem of natural convection because the duration of the experiment is short compared with the time for the onset of significant heat transfer associated with the inevitable flow. Another important feature is that this new technique works in accord with a theoretical model, which enables absolute measurements to be made with an uncertainty of $\pm 2\%$ in the final value for the thermal conductivity. In this paper the technique and the instrument constructed according to this technique will be presented, while in a subsequent paper [5], the results of measurements of the thermal conductivity for four molten metals will be reported.

2. THEORETICAL

The method is based on the transient hot-wire technique [6]. In the typical version of this technique a vertical wire is suspended in the test fluid and the temperature rise of the wire is measured as a function of time after initiation of a heat pulse within it. The temperature rise is followed by measuring the resistance change of a finite section of the wire. However, in the current work we are applying this technique for the measurements of electrically conducting materials; it is therefore necessary to encase the wire in an electrical insulator. The ideal concept of the method envisages an electrically conducting material with density ρ_w, isobaric heat capacity C_{Pw}, and thermal conductivity λ_w and of infinite extent in the axial-direction placed symmetrically in the middle of the substrate material of density ρ_s, isobaric heat capacity C_{Ps}, and thermal conductivity λ_s, which is itself immersed in the molten material with density ρ_m, isobaric heat capacity C_{Pm}, and thermal conductivity λ_m which is infinite in the x, y, and z directions as shown in Fig. 1. It can be seen in this figure that the hot wire is represented by a square centered on the origin. In practice the wire cross section is circular, but the use of the square section avoids the difficulty of a mixed geometry

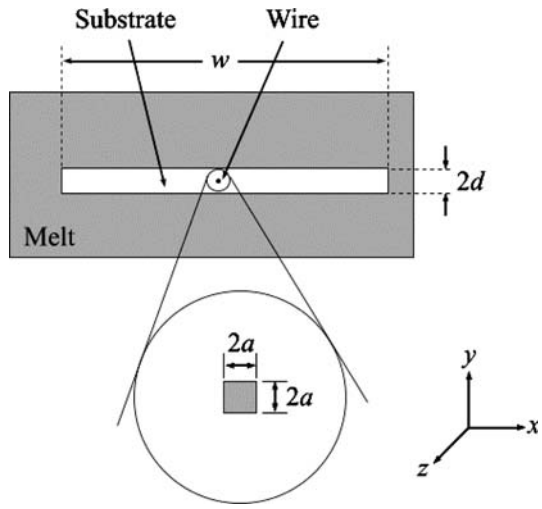

Fig. 1. Ideal concept of the method.

and reduces the computational time for the solution of the working equations resulting from a careful mathematical model of the instrument. Independent calculations [7] confirm that the distinction between the behavior of a wire of square cross section and of a wire of circular cross section is entirely negligible on the time scale of interest.

A constant heat flux per unit length q is generated within the wire from time $t=0$. The wire is initially in equilibrium with the substrate and the melt at a temperature T_0 at time $t=0$. The heating causes the temperature of the wire to increase which, in turn, alters the resistance of each section of the wire as a function of time. The temperature rise is determined by the thermophysical properties of the wire ($\rho_w, C_{pw}, \lambda_w$), the substrate ($\rho_s, C_{ps}, \lambda_s$), and the melt ($\rho_m, C_{pm}, \lambda_m$). The resistance change of a central section of the wire is recorded by an automatic bridge and converted to a temperature rise by an independent calibration of the temperature resistance of the wire.

2.1. Working Equations

The formulation of the working equations is derived from the solution of the conservation of energy equation for a viscous, isotropic, and incompressible material with temperature independent properties. On the assumption that the perturbation of the temperature is small and that a local-equilibrium thermodynamic state exists, this solution becomes [6, 8]

$$\rho C_p \frac{\partial T}{\partial t} = \lambda \nabla^2 T. \tag{1}$$

In the above equation, ρ is the density, C_p is the isobaric heat capacity, T is the absolute temperature, t is the time, and λ is the thermal conductivity. This equation is the basis of all transient experimental methods for the measurement of thermal conductivity, and it can be applied to the three distinct regions of this model: the wire, the substrate, and the melt. The result of Eq. (1) for the three different regions in the present system gives the following set of coupled partial differential equations:
for the wire:

$$\rho_w C_{Pw} \frac{\partial T_w}{\partial t} = \lambda_w \left[\frac{\partial^2 T_w}{\partial x^2} + \frac{\partial^2 T_w}{\partial y^2} \right] + \frac{q}{a^2} \tag{2}$$

for the substrate material:

$$\rho_s C_{Ps} \frac{\partial T_s}{\partial t} = \lambda_s \left[\frac{\partial^2 T_s}{\partial x^2} + \frac{\partial^2 T_s}{\partial y^2} \right] \tag{3}$$

for the melt:

$$\rho_m C_{Pm} \frac{\partial T_m}{\partial t} = \lambda_m \left[\frac{\partial^2 T_m}{\partial x^2} + \frac{\partial^2 T_m}{\partial y^2} \right] \tag{4}$$

If the transient heating is begun at $t = 0$ when the temperature is uniform everywhere, then it follows from Fig. 1 that the solution of these equations is subject to the following initial condition for $t = 0$:

$$T_w = T_s = T_m = T_o, \quad \text{for all } x, y \tag{5}$$

and the following boundary conditions in the ideal case for $t > 0$:

(a) for the wire-substrate interface
when $y = \pm a$, $x = 0$ to $\pm$a and $x = \pm a$, $y = 0$ to $\pm a$,
then

$$T_w = T_s \tag{6}$$

and

$$\lambda_w \frac{\partial T_w}{\partial x} = \lambda_s \frac{\partial T_s}{\partial x} \tag{7}$$

$$\lambda_w \frac{\partial T_w}{\partial y} = \lambda_s \frac{\partial T_s}{\partial y} \tag{8}$$

(b) for the substrate-melt interface
when $y=-d, \quad x=0 \text{ to } \pm w/2$ and $y=d, \quad x=0 \text{ to } \pm w/2$,
then

$$T_m = T_s \tag{9}$$

and

$$\lambda_m \frac{\partial T_m}{\partial x} = \lambda_s \frac{\partial T_s}{\partial x} \tag{10}$$

$$\lambda_m \frac{\partial T_m}{\partial y} = \lambda_s \frac{\partial T_s}{\partial y} \tag{11}$$

(c) while

$$\text{for } x \to \infty \text{ or } y \to \infty \quad T_m = T_o \quad t > 0 \tag{12}$$

Since there is no available analytical solution for the present working equations, it is necessary either to devise an approximate model to represent reality in a manner that allows an analytical solution, or to use a numerical procedure. In this work we decided to use a numerical procedure; thus, a specialized two-dimensional finite element (2D-FEM) program for the solution of these equations was developed. A total of 441 elements in a 2D-rectangular variable size mesh were employed. The mesh within the wire and in the interfaces is quite dense, with the elements' size increasing inside the melt the further they are located from the interface. The suitability of the representation of the circular wire as a mesh of rectangular elements has been carefully examined and discussed elsewhere [7].

2.2. FEM Program Validation

There is no direct way to validate the 2D-FEM program we have employed because there is no other solution to the same problem available. For that reason we have developed a one-dimensional finite element (1D-FEM) program. This simulates the temperature rise of the wire with circular geometry immersed in an infinite body of substrate material alone, and it is compared with the exact solution for this problem given by Carslaw and Jaeger [9]. This same analysis can also be employed, of course, to demonstrate the accuracy of the use of a square geometry to simulate the wire [7].

Simulations were carried out up to 1 ms. Before this time only the wire and the substrate participate in the heat transfer process, so that only the thermophysical properties of the substrate material and the wire are required

for both calculations. To compare the temperature rise data obtained with both solutions, a deviation plot of the 1D-FEM solution from the exact analytical solution (denoted by theory [6]) is given in Fig. 2.

The very small discrepancies observed between theory and 1D-FEM are within 0.2% at all times and are substantially constant after about 0.1 ms. This is adequate agreement to encourage the use of a FEM for the description of our experimental method because the discrepancies are commensurate with the precision that can be achieved in the experimental measurement of the temperature rise.

Subsequently, the 2D-FEM program was employed to solve exactly the same problem and the results compared with that for the one-dimensional solution. Differences between the two solutions were found only for times less than 10 μs when the square shape assumed for the 2D version of the source differs from the cylindrical symmetry. For larger times the difference becomes very small, so that by 1 ms and beyond, it is negligible. In particular, for the case of the determination of the thermal conductivity of the melt, which is obtained from long times ($t > 10$ ms), the cross section of the wire has an insignificant effect.

The 2D-FEM program can thus be used to calculate the temperature rise of the wire in an experiment where the thermophysical properties of the wire, the substrate, and the melt are known. The thermal conductivity of the melt can be obtained from such an experiment if we know the remainder of the properties for the system and the dimensions of all components, by varying the thermal conductivity to obtain a match between the experimental and calculated temperature rise at long times, > 10 ms. In

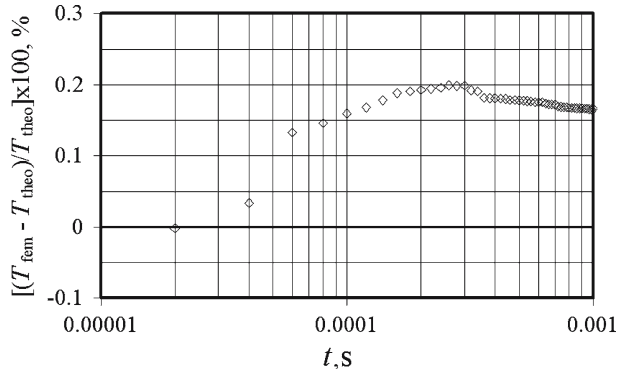

Fig. 2. Deviation of the temperature rise obtained using the 1D-FEM from that obtained from the solution given by Carslaw and Jaeger [9].

fact, because the entire temperature rise as a function of time is obtained in such detail, some of the other properties can also be obtained from the experimental data *in situ*, as is described in the following sections.

3. EXPERIMENTAL

3.1. Sensor

The design of the sensor is shown in Fig. 3. It has been fabricated using 96% pure green alumina substrate, and the sensing element has been made from a wire of 25 μm diameter of 99.99% pure platinum. The connections to the wire have been printed directly on the top of one sheet of green alumina of dimensions 100 mm length, 58 mm width, and 0.4 mm thickness, using platinum ink and a screen printing technique [8]. Platinum foils of 99.99% purity are attached at each end of the connections, and a second sheet of alumina is then placed on top of it. The sandwich is then hot pressed at 180°C for 20 min at 350 $kg \cdot cm^{-2}$ in order to guarantee the best contact between the substrate and the platinum wire. After pressing, the entire assembly is placed in a programmable high temperature furnace and baked with an appropriate temperature profile up to 1600°C. This process yields a rectangular, rigid sensor 85 mm long, 50 mm wide, and approximately 650 μm thick.

To facilitate the connection of the sensor to the measurement system, nickel wires 0.5 mm in diameter and of 99.98% purity (temper as hard), supplied by Goodfellow, are spot-welded to each of the platinum leads of the sensor (see Fig. 4). To protect the connections, two pieces of fired alumina plates are glued to the sensor using a Chromix 2-part chemical setting adhesive (supplied by Fortafix). Between the two pieces of alumina, two nickel wires were attached at each side for the sensing of the level of the

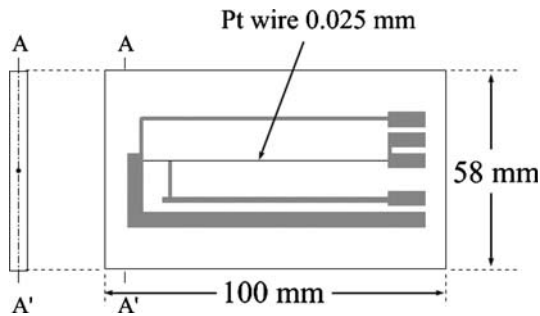

Fig. 3. Platinum-wire sensor.

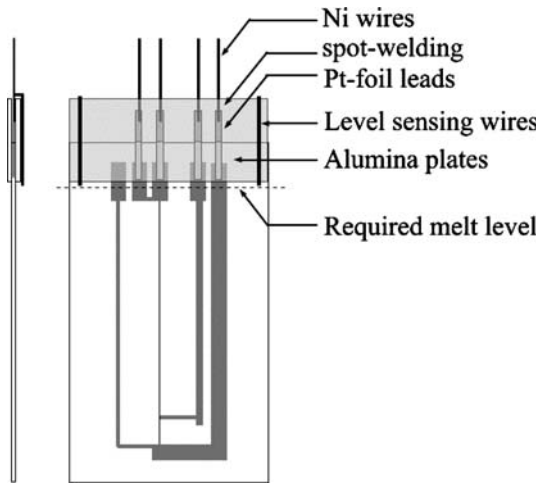

Fig. 4. Platinum-wire sensor with connector leads.

molten metal in which the sensor is immersed. It is essential that the molten material cover more than half of the upper connections of the wire.

The sensor is then mounted on a thin-walled metal tube which is itself mounted through the top sealing cap of a high-temperature furnace as shown in Fig. 5. The tube passes through a seal in the top cap of the furnace that is provided with a controlled atmosphere of argon with a purity of 99.999 %. The top cap is water-cooled to prevent damage to the seal.

The liquid metal, which is contained in an alumina crucible, is placed inside the furnace on a pneumatically operated table which is mounted coaxially with the sensor but below it. The table allows the crucible to be raised around the sensor for measurement, but to be withdrawn between measurements in order to limit any chemical reaction between the sensor and melt. An extra heater is mounted on the tube that carries the sensor in order to ensure the temperature of the tube is about 1°C above the melt temperature so that there is a stable density profile and convection currents are eliminated. The wires connecting to the sensor, the heater, and the thermocouples pass through the middle of the tube that suspends the sensor.

The measurement of the temperature in the furnace is performed by an automatic/programmable Eurotherm controller Model 1904. Since the measurements performed during this work were below 500°C, a thermocouple of type K in a stainless steel sheath is embedded in the chamber at the middle of the furnace for the measurement of its temperature. The temperature of the melt is measured by a thermocouple immersed in the melt at the time of measurement at three different positions, at the

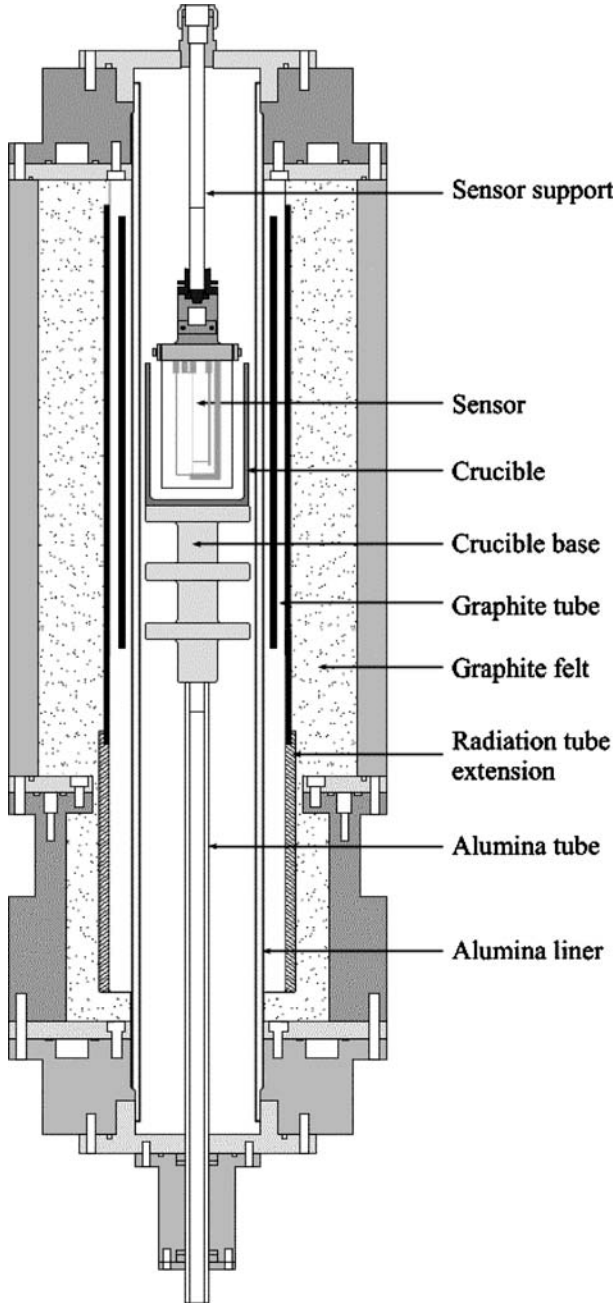

Fig. 5. Assembly of the sensor in the furnace.

bottom, the middle, and the surface, assuring the same temperature along the sample. The control of the inert gas is achieved using two Low Flow indicators Model LFC 1510, and the flow line exits through an appropriate cold trap to prevent the egress of metal vapor.

In order to perform measurements, the metal is melted from solid in the crucible, placed within the furnace. The level of liquid in the crucible is detected using the detection system described earlier. If further metal is needed to increase the level, it can be added through the tube carrying the sensor. In use, the crucible is slightly above the middle of the furnace so that the best temperature distribution over the sensor is achieved. In this way, it is possible to achieve a uniform temperature environment around the sample within ± 0.1 K.

An additional important determination of the temperature distribution is provided by continuous monitoring of the resistance of the thermal conductivity sensor at a nominal steady state. If there is a convective flow within the melt under such conditions the sensitivity of the bridge measurement system reveals small oscillations in the temperature of the sensor. Absence of such fluctuations confirms a stable temperature distribution prior to measurements.

3.2. Bridge

The measurements consist of transient heating of the platinum wire by the application of heat generation within it and subsequent measurement of the resistance change of a part of the wire. To accomplish this, we developed a Wheatstone electronic bridge circuit to generate a constant heat flux within the wire and to monitor its change of resistance with an uncertainty of $\pm 0.1\%$ during 1 s. The technique is designed to eliminate, at the same time, the end effects. The temperature rise of the wire is calculated from temperature-resistance characteristics of the hot wire using a prior calibration. This bridge allows measurements of temperature rises at times as short as $20\,\mu$s after the application of the transient and subsequently at two different acquisition rates which provide a large number of data points for use in the data fitting process outlined earlier.

The bridge circuit, shown in Fig. 6, has been designed to measure the evolution of the resistance change of a finite portion of an infinite wire, by automatically compensating for wire ends, and to generate a nearly constant heat flux in the hot wires of known magnitude. In this section, the working bridge equations are derived from an analysis of the circuit.

The diagram shows schematically two wires, one short and one longer, denoted by R_S and R_L, respectively. The wires are assumed to be

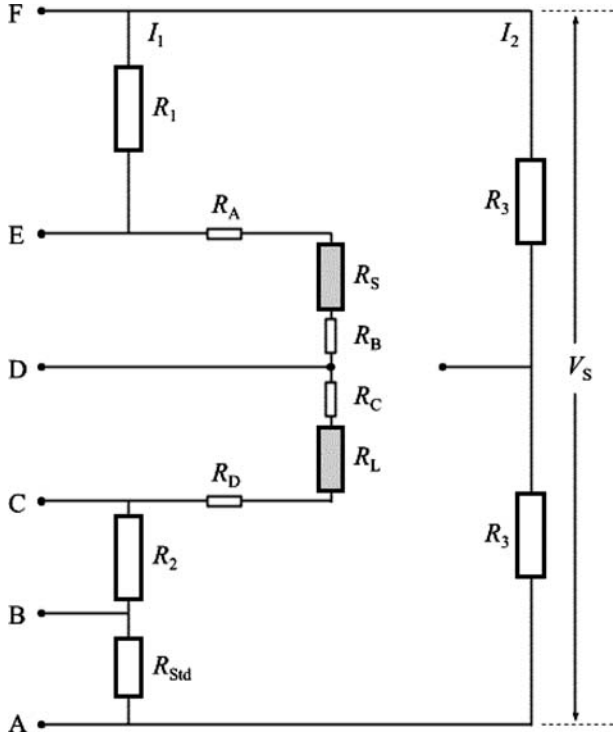

Fig. 6. Electronic bridge diagram.

identical in all respects except for length. The two components are formed by two sections of a single wire divided by a potential tap. The bridge is arranged so as to determine the difference of resistance between the two parts of the same wire. In this way, we eliminate from the measurements the effects of the ends of the wire where the temperature rise is not uniform as a result of the connections. This compensation is exact if the short wire is sufficiently long and the wires identical. The condition upon the length has been tested experimentally, and the tests are described elsewhere [7, 8]. It is usual, but not essential, to ensure that the resistances of the wire connections in the bridge,

$$R_A + R_B = R_C + R_D; \tag{13}$$

then, by analyzing the bridge circuit, the expression for the change in resistance of a hypothetical segment of an infinite 'working' wire $\Delta R_W(t) = R_W(t) - R_W(0)$ as a function of time t can be expressed as [7]

$$\Delta R_{\mathrm{W}}(t) = \frac{\frac{\Delta V_{\mathrm{AD}}(t)}{V_S}[\Sigma R(0)]^2}{\left[\Sigma R(0)\left(1+\frac{R_{\mathrm{S}}(0)}{R_{\mathrm{W}}(0)}\right) - R_{\mathrm{F}}(0)\left(1+2\frac{R_{\mathrm{S}}(0)}{R_{\mathrm{W}}(0)}\right) - \frac{\Delta V_{\mathrm{AD}}(\mathrm{t})}{V_{\mathrm{S}}}\Sigma R(0)\left(1+2\frac{R_{\mathrm{S}}(0)}{R_{\mathrm{W}}(0)}\right)\right]}, \tag{14}$$

where $R_{\mathrm{W}}(t)$ and $R_{\mathrm{W}}(0)$ denote the resistance of the 'working' wire at any time and at zero time ($t=0$), respectively, defined as

$$R_{\mathrm{W}}(t) = R_{\mathrm{L}}(t) - R_{\mathrm{S}}(t) \tag{15}$$

and

$$R_{\mathrm{W}}(0) = R_{\mathrm{L}}(0) - R_{\mathrm{S}}(0). \tag{16}$$

In the above equations, $R_{\mathrm{L}}(t)$ and $R_{\mathrm{L}}(0)$ are the resistances of the long wire at time t and at zero time ($t=0$), $R_{\mathrm{S}}(t)$ and $R_{\mathrm{S}}(0)$ are the resistances of the short wire at time t and at zero time ($t=0$), $\Delta V_{\mathrm{AD}}(t)$ is the measured out-of-balance voltage, across points A to D in Fig. 6 and V_{S} is the supply voltage. $\Sigma R(0)$ is the sum of the resistances of the left-hand side of the circuit at zero time, expressed as

$$\Sigma R(0) = R_1 + R_{\mathrm{A}} + R_{\mathrm{S}}(0) + R_{\mathrm{B}} + R_{\mathrm{C}} + R_{\mathrm{L}}(0) + R_{\mathrm{D}} + R_2 + R_{\mathrm{Std}}, \tag{17}$$

and $R_{\mathrm{F}}(0)$ is the sum of the bottom arm resistances,

$$R_{\mathrm{F}}(0) = R_{\mathrm{C}} + R_{\mathrm{L}}(0) + R_{\mathrm{D}} + R_2 + R_{\mathrm{Std}}. \tag{18}$$

Equation (14) implies that by implementing the present bridge design, shown in Fig. 6, it is possible to calculate the resistance change for a hypothetical segment of an infinite wire with a knowledge of the following information:

(a) the ratio of the out-of-balance voltage and the supply voltage $\Delta V_{\mathrm{AD}}(t)/V_{\mathrm{S}}$ at time t,

(b) the total resistance of the left-hand arm of the circuit $\Sigma R(0)$ and the bottom arm resistance $R_{\mathrm{F}}(0)$ at zero time, and

(c) the ratio of the short to the 'working' wire resistance $R_{\mathrm{S}}(0)/R_{\mathrm{W}}(0)$ at zero time.

Finally, we note that the values of the unknown resistances $\Sigma R(0)$, $R_{\mathrm{F}}(0)$, $R_{\mathrm{L}}(0)$, $R_{\mathrm{S}}(0)$, R_1, and R_2 required are all calculated in relation to the known value of the standard resistor R_{Std}, by registering the corresponding voltages. Values of the lead resistance are measured during the assembly of the sensor and its connections.

The above analysis assumes the generation of a constant heat flux within the long and short wires. The implication in this statement is that the same constant current must therefore flow through both wires. Since the resistance of both wires is changing with time, the current also necessarily changes. However, the change in the resistance difference of the two wires, over a single-measurement interval, is of the order of $10^{-3}\,\Omega$. This corresponds to a change of current, of the order of $10^{-6}\,\mathrm{A}$ (assuming $\Sigma R(0) \approx 50\,\Omega$., and $V_S \approx 5\,\mathrm{V}$), which in turn results in a change of the heat flux per unit length of the order of $10^{-6}\,\mathrm{W}\cdot\mathrm{m}^{-1}$ (when typical values of heat flux per unit length employed are about $3\,\mathrm{W}\cdot\mathrm{m}^{-1}$). Hence, both the heat flux per unit length and the current can safely be considered as constants.

Thus, the same current I_1 flows through both wires. Analyzing the bridge circuit, it can be shown that the heat flux per unit length of the middle portion of the long wire, at any instant t, can then be expressed as

$$q = \frac{V_S^2}{\left\{R_1 + R_A + R_B + R_C + R_D + R_2 + R_{Std} + \frac{R_W(t)(L_L+L_S)}{L_L-L_S}\right\}^2} \frac{R_W(t)}{L_L - L_S} \tag{19}$$

where L_L and L_S are the lengths of the long and short wires, respectively. Finally, we should note that as a result of the manufacturing process of 'thin' hot wires (and the wire supports), it is difficult to ensure that the cross section of the two wires is uniform, which may result in a small variation in the resistance per unit length of the wires. A small correction is hence applied to the measured temperature rise and heat flux, as described elsewhere [10].

3.3. Temperature Coefficient of Resistance

The temperature rise of the central section of the wire, $\Delta T = T(t) - T_0$, can be calculated from resistance measurements with the aid of the following equations. The resistance of the wire at $t = 0$ is

$$R_w(0) = R_0 \left\lfloor 1 - \alpha(T_0 - 273.15) + \beta(T_0 - 273.15)^2 \right\rfloor \tag{20}$$

where T_0 is the measured temperature at time $t = 0$, R_0 is the resistance of the wire at 273.15 K, and α and β are the first and second temperature-resistance coefficients of the platinum wire. At time t when the temperature is T, we can use, equivalently,

$$R_w(t) = R_0 \left\lfloor 1 - \alpha(T - 273.15) + \beta(T - 273.15)^2 \right\rfloor \tag{21}$$

Measurements of $R_w(t)$ and R_0 allow the evaluation of the temperature rise at time t. The coefficients α and β, obtained under calibration, were found to be equal to $3.992 \times 10^{-3}\,\mathrm{K}^{-1}$ and $-8.8512 \times 10^{-7}\,\mathrm{K}^{-2}$, respectively. The aforementioned values are in full agreement with the recommended values for pure platinum.

3.4. Validation of the Technique

To validate the technique, an experimental run was carried out in mercury at room temperature. For the calculation of the theoretical temperature rise using the 2D-FEM program, we used the known values of ρ, C_P of platinum [11], alumina [12] and mercury [13–18] and the thermal conductivity of platinum [11], as well as, assumed values of the thermal conductivity for alumina and mercury. We also employed the measured dimensions of the sensor and the wire and the value of q used during an experiment. Because the different materials influence the temperature rise over quite different time scales, it is possible in this way to obtain independent values of the thermal conductivity of the melt and of the alumina substrate *in situ*.

Figure 7 is a schematic representation of the measured and simulated temperature rises where it can be seen how the temperature rise of the wire is affected by the thermophysical properties of the different materials at different times. For very short times, $t < 100\,\mu\mathrm{s}$, the temperature rise of the wire is affected only by the thermophysical properties of the

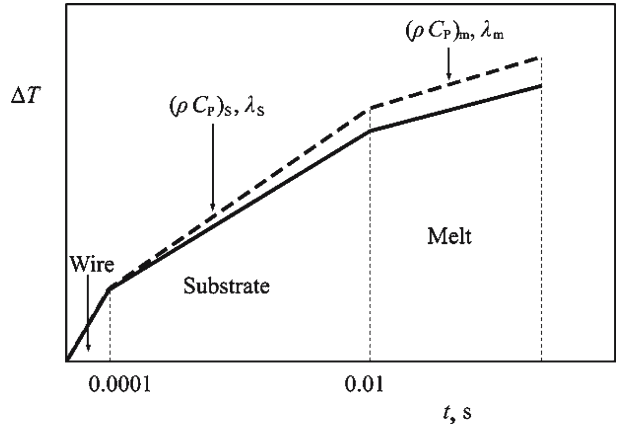

Fig. 7. Schematic representation of the measured and simulated temperature rises as a function of time.

platinum wire, whereas, for longer times, $t < 10\,\text{ms}$, it is affected by the thermophysical properties of the alumina substrate. For even longer times, $t > 10\,\text{ms}$, the temperature rise depends also on the properties of the melt. Therefore, to minimize the differences at times $t < 10\,\text{ms}$, we have to adjust the thermal conductivity of the alumina substrate, and for times $t > 10\,\text{ms}$, the thermal conductivity of the melt. Once the optimal agreement between measured and simulated temperature rise data is obtained, the values of the thermal conductivity of the alumina and melt that best represent the experimental temperature rise are the measured values corresponding to the reference temperature [19] of that measurement.

To compare the agreement between measured and simulated temperature rise data, the differences between them ($T_{\text{exp}} - T_{\text{sim}}$) are plotted against time in Fig. 8. The plot shows that at very short times, $t \leqslant 100\,\mu\text{s}$, there are systematic deviations between experiment and simulation that are small (0.05 K) but significant. There is then good agreement between calculation and experiment up to 10 ms when again a step change in the deviation takes place. After 100 ms there is again accord between experiment and simulations in the sense that the lines are parallel but there is a distinct temperature shift between them.

This analysis leads us to the conclusion that the theoretical model can closely represent the heat transfer process within the alumina and within the melt separately, but that between them, it has failed to give a proper representation of the interfaces between the platinum wire and substrate and between the substrate and melt. This behavior can readily be explained in terms of the discontinuity at the interface between the two materials at the atomic level. That is, the ideal boundary conditions at the interfaces set out earlier in Eqs. (10) to (15) are not satisfied by the real interfaces.

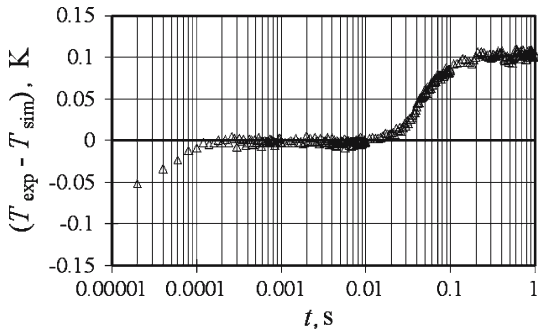

Fig. 8. Comparison between measured and simulated temperature rise data for mercury.

To analyze this hypothesis, we first introduced into our finite element model a heat transfer resistance at the interface between the platinum wire and alumina substrate, this heat transfer resistance is represented by a layer L1, with thermophysical properties λ_{L1}, ρ_{L1}, C_{pL1}, and thickness b. We have assumed the properties to be those of air and varied the thickness, but we also verified that the exact nature of the layer does not matter; the use of different thermophysical properties leads to a different layer thickness for the same optimal reproduction of the experiment. Figure 9 is a representation for the analysis of the layer, L1, at the platinum wire-substrate interface which is not to scale. The figure shows only the platinum wire and alumina where their dimensions have been exaggerated in order to give a better illustration to support the development of the new equations to model the experiment at short times $t < 10$ ms. The equations developed for the new layer L1 and the new boundary conditions are given below.

The equations for the platinum wire and the alumina region have been shown already, thus, here we present only the equation for the new layer L1;

$$\rho_{L1} C_{P_{L1}} \frac{\partial T_{L1}}{\partial t} = \lambda_{L1} \left[\frac{\partial^2 T_{L1}}{\partial x^2} + \frac{\partial^2 T_{L1}}{\partial y^2} \right], \tag{22}$$

subject to the following initial and boundary conditions:

(a) initial conditions for $t = 0$

$$T_w = T_{L1} = T_s = T_m = T_0, \qquad \text{for all } x, y \tag{23}$$

(b) Boundary conditions for $t > 0$

(i) for the wire-L1 interface
when $y = \pm a$, $x = 0$ to $\pm a$ and $x = \pm a$, $y = 0$ to $\pm a$, then

$$T_w = T_{L1} \tag{24}$$

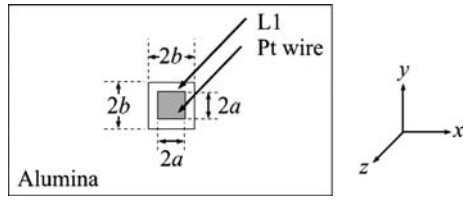

Fig. 9. Schematic representation of the platinum wire-substrate interface.

and

$$\lambda_w \frac{\partial T_w}{\partial x} = \lambda_{L1} \frac{\partial T_{L1}}{\partial x} \tag{25}$$

$$\lambda_w \frac{\partial T_w}{\partial y} = \lambda_{L1} \frac{\partial T_{L1}}{\partial y} \tag{26}$$

(ii) for L1-substrate interface
when $y = \pm b$, $x = 0$ to $\pm b$ and $x = \pm b$, $y = 0$ to $\pm b$, then

$$T_s = T_{L1} \tag{27}$$

and

$$\lambda_s \frac{\partial T_s}{\partial x} = \lambda_{L1} \frac{\partial T_{L1}}{\partial x} \tag{28}$$

$$\lambda_s \frac{\partial T_s}{\partial y} = \lambda_{L1} \frac{\partial T_{L1}}{\partial y} \tag{29}$$

This new set of equations has been included in the 2D-FEM program, and new simulations carried out up to 10 ms for a range of values of b. This process allows the analysis of only the heat transfer process between the platinum and the alumina, but including now the new heat transfer resistance in the layer L1. It is possible by variation of the layer thickness to obtain secure improved agreement between experiment and theory in this region. Figure 10 shows that the inclusion of the new layer allows considerable improvement of the representation of the behavior of the sensor at short times. The thickness of the layer (b–a) found to yield optimum agreement in the experiment is 5 nm, which is entirely plausible.

Using this result it is also now possible to analyze the sensitivity of the technique to the thermal conductivity of alumina. To conduct this analysis, the thermal conductivity of alumina was changed by $\pm 2\%$ around the optimal value and the calculations of the temperature rise repeated for each case. Figure 11 shows the comparison between measured and calculated temperature rises of the wire up to 10 ms. Here it can be seen that it is straightforward to distinguish a change of the thermal conductivity of the alumina of $\pm 2\%$ and that the optimal thermal conductivity of alumina at 295.6 K is 25.2 $W \cdot m^{-1} \cdot K^{-1}$. The latter value is comfortably within the range that can be found in the literature for alumina 96% at this temperature.

It has been shown so far that the theoretical model with the inclusion of the heat transfer resistance at the platinum–alumina interface can give excellent agreement between experiment and theory up to 10 ms and that the thermal conductivity of the substrate can be obtained with a precision of ±2%. It is important now to prove that the same value for the thermal conductivity of alumina is appropriate when studying different fluids at the same temperature. Evidently, if the model employed is appropriate, the fluid studied should have no effect on the measured properties of the alumina. Equally, the same analysis can be also used to demonstrate that the physical properties of the interface region (λ, ρ, C_p, b) of layer L1 are not affected by the properties of the melt and that the value remains constant for the two different experiments at the same temperature.

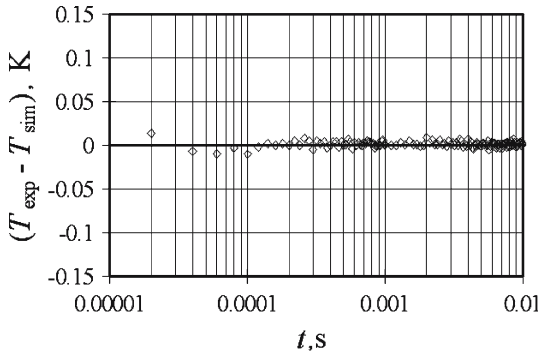

Fig. 10. Comparison between measured and simulated temperature rise data with an interface heat transfer resistance between the platinum wire and alumina substrate.

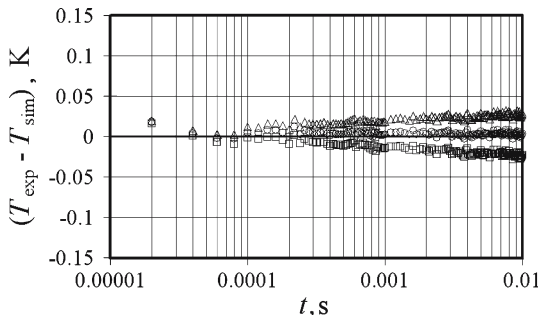

Fig. 11. Effect of the thermal conductivity of alumina (◯) $\lambda_{Al} = 25.2\,W \cdot m^{-1} \cdot K^{-1}$; (△) $\lambda_{Al} = 25.71\,W \cdot m^{-1} \cdot K^{-1}$ (+2%); (□) $\lambda_{Al} = 24.69\,W \cdot m^{-1} \cdot K^{-1}$ (−2%).

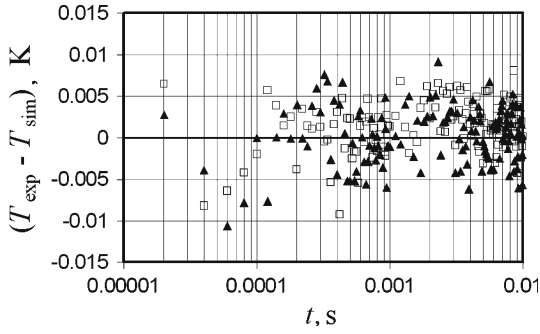

Fig. 12. Comparison between measured and simulated temperature rise data of alumina for measurements (▲) in mercury and [□] in gallium at 333 K.

For this purpose, measurements were carried out using mercury and gallium at a temperature of about 333 K and at atmospheric pressure. Figure 12 shows, on a larger scale, a comparison between the measured and simulated temperature rises of the wire for the time scale when just the alumina properties are involved in the heat transfer process ($t < 10$ ms). The thermal conductivity of alumina which provides the optimum description of the two different experiments for two different molten metals is $22.1\,\mathrm{W \cdot m^{-1} \cdot K^{-1}}$, which is within the range of values reported in the literature for alumina 96 % at this temperature. It is also exceedingly important to note that the thickness of the layer of heat transfer resistance at the platinum–alumina interface in the calculations for both molten metals is identical and is also identical with that used for calculations using mercury at room temperature. These results confirm the model is adequate to treat the heat transfer resistance between the platinum and the alumina substrate.

Figure 9 illustrated that as well as a heat transfer resistance at the interface between the platinum wire and the alumina substrate, a similar resistance arose at the surface between the substrate and the molten metal. To account for this resistance we have added a second layer with properties similar to those used for the platinum–alumina interface at the alumina substrate–melt interface. Similar equations, as in the previous case, were derived and included in the 2D-FEM program [19]; they are not repeated here in the interests of brevity. Simulations were carried out again for an experiment in mercury at room temperature. In these simulations the thickness of this layer was varied in order to secure optimal agreement between experiment and theory. Figure 13 shows a comparison between the measured and simulated temperature rise of the wire for the optimal thickness thus obtained. This figure confirms that with the implementation of the new

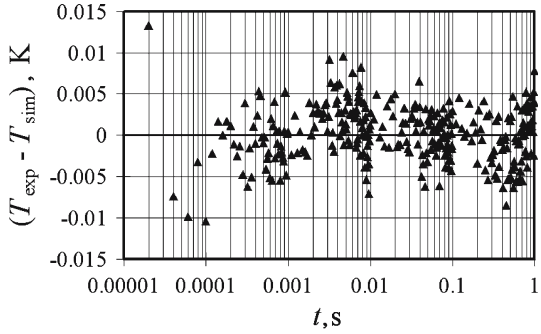

Fig. 13. Comparison between measured and simulated temperature rise data with heat transfer resistance at interfaces of platinum wire–alumina substrate and alumina substrate–melt.

set of equations at platinum wire–alumina and alumina–melt interfaces it is possible to obtain a theoretical description of the real behavior of the sensor over the entire time range during an experiment in one fluid at one temperature. It can be seen also that the deviation seldom exceeds about 0.1% of the temperature rise and that it is essentially randomly distributed about zero over five decades of time during which the heat pulse transverses three different materials. This is strong evidence that the theoretical model is a faithful representation of the real sensor and that the precision of the temperature measurement is of the order of 0.1%. It should be noted further that the thickness of the layer required to secure this agreement is 0.3 μm which is again an entirely plausible value. However, it is expected that this thickness may change slightly from melt to melt since it is likely to depend upon the physicochemical properties of the melt.

It should be mentioned that the heat transfer process for our hot-strip sensor is more complicated than that for the conventional hot wire for reasons beyond the altered symmetry and geometry. The existence of several solid materials in the sensor itself, inevitably lead to discontinuities in temperature at the interfaces. Furthermore, the liquid–solid interface is very different between the circumstances for molten metals next to an alumina interface, from an organic liquid adjacent to a platinum wire. The wetting properties of the fluids and surface in the current work and the very high difference in thermal conductivity of the metal lead to similar discontinuities at the solid–molten metal interface.

To analyze the sensitivity of the technique to the thermal conductivity of mercury, simulations were carried out varying the value of the thermal conductivity of mercury by ±1% around the value which provides the best representation of the data. Figure 14 shows the results obtained, where it

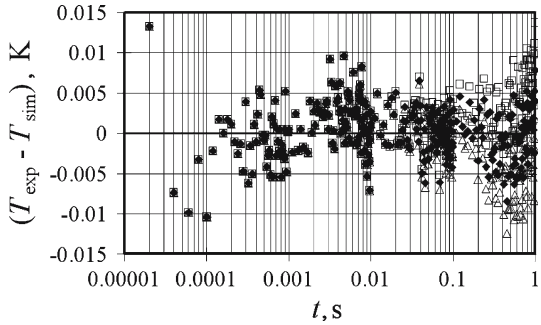

Fig. 14. Effect of the thermal conductivity of mercury: (♦) $\lambda_{Hg} = 8.05\,W \cdot m^{-1} \cdot K^{-1}$; (△) $\lambda_{Hg} = 7.96\,W \cdot m^{-1} \cdot K^{-1}(-1\,\%)$; (□) $\lambda_{Hg} = 8.13\,W \cdot m^{-1} \cdot K^{-1}(+1\,\%)$.

can be seen that the differences in the fit arising from this small change in the thermal conductivity of the melt can be easily discerned. The same chart can also be used to support the statement made earlier that the thermal conductivity of the melt affects only the very long times of the temperature rise of the wire, $t > 10$ ms, and has no effect upon the heat transfer process inside the sensor. After $t > 10$ ms the fit to the experimental data achieved by the perturbed values of the thermal conductivity of the melt is discernibly worse than for the optimal value. From this analysis is possible to assert that the thermal conductivity of mercury at 295.6 K is $8.05\,W \cdot m^{-1} \cdot K^{-1}$, which is a value comparable with those reported in the literature for this temperature by other authors [20–25].

3.5. Precision and Accuracy

The preceding discussion has provided strong evidence that the heat transfer model developed for the description of the insulated hot-wire sensor is entirely consistent with the practical operation of the sensor over a time range of five orders of magnitude as the heat pulse transmits through three different materials. The analysis has also shown that with the temperature resolution available from the resistance bridge, $\pm 0.1\,\%$, it is possible to distinguish the thermal conductivity of the melt to within $\pm 1\,\%$. Allowing for errors in the calibration of the resistance–temperature characteristics of the platinum wire, the effects of uncertainties in the dimensions of the sensor and in the remaining physical properties of the system, determined by simulation, it is possible to assert that the uncertainty in the thermal conductivity of the molten metals determined by this technique is $\pm 2\,\%$.

4. CONCLUSIONS

In this paper the instrumentation for the measurement of the thermal conductivity of molten metals at high temperature has been described together with a mathematical model that faithfully represents its behavior. Evidence has been adduced to support the consistency between the theoretical model and the practical operation of the sensor. It is important to emphasize that the new technique can, in principle, be applied to the measurement of the thermal conductivity of any molten material; however, in this particular work, the sensor has been constructed and restricted for measurements on molten materials with a thermal conductivity above $8\,W \cdot m^{-1} \cdot K^{-1}$. This is mainly due to the properties and thickness of the substrate material employed. In this case the thickness of the alumina is relatively large ($> 500\,\mu m$) with a relatively low thermal conductivity that tends to decrease when the temperature increases. Thus, if the test sample is a poorly conducting material, the substrate prevents heat transfer from the wire to the fluid and the latter barely affects the evolution of the temperature of the wire. Therefore, for measurements of low thermal conductivity materials, the sensor must be modified so that a thinner substrate material with higher thermal conductivity over the temperature range of interest is employed. A second paper [5] applies the instrument described here to the measurement of the thermal conductivity of mercury, gallium, tin, and lead over a range of temperatures.

REFERENCES

1. R. Tufeu, J. P. Petitet, L. Denielou, and B. Le Neindre, *Int. J. Thermophys.* **6**:315 (1985).
2. Y. Nagasaka and A. Nagashima, *Int. J. Thermophys.* **12**:769 (1991).
3. N. Nagazawa, Y. Nagasaka, and A. Nagashima, *Int. J. Thermophys.* **13**:753 (1992).
4. E. P. Sakonidou, M. J. Assael, C. A. Nieto de Castro, H. R. van den Berg, and W. A. Wakeham, *Thermal Conductivity* **24**:516 (1999).
5. M. V. Peralta-Martinez, M. J. Assael, M. Dix, L. Karagiannidis, and W. A. Wakeham, submitted to *Int. J. Thermophys* (in press).
6. M. J. Assael, C. A. Nieto de Castro, H. M.Roder, and W. A. Wakeham, "Transient Methods for Thermal Conductivity," Chap. 7 in *Experimental Thermodynamics, Vol. III, Measurement of the Transport Properties of Fluids*, A. Nagashima, J. V. Sengers, and W. A. Wakeham, eds. (Blackwell Scientific, Oxford, 1991), pp. 161–195.
7. M. J. Assael, M. Dix, K. Gialou, L. Vozar, and W. A. Wakeham, *Int. J. Thermophys.* **23**:615 (2002).
8. M. Dix, I. W. Drummond, M. Lesemann, M. V. Peralta-Martinez, W. A., Wakeham, M. J. Assael, L. Karagiannidis, and H. R. van den Berg, *Proc. 5th Asian Thermophysical Properties Conference*, Seoul, Korea (1998), p. 113.
9. H. S. Carslaw and J. C. Jaeger, *Conduction of Heat in Solids*, 2nd Ed. (Oxford University Press, 1959).
10. J. Kestin and W. A. Wakeham, *Physica A* **92**:102 (1978).

11. *Handbook of Chemistry and Physics*, 76th Ed. (CRC Press, Boca Raton, Florida, 1995–1996).
12. W. D. Kingery and M. C. McQuarrie, *J. Am. Ceram. Soc*. **37**:107 (1954).
13. F. Simon, *Ann. Physik* **68**:241 (1922).
14. A. L. Dixon and W. A. Rodebusch, *J. Am. Chem. Soc*. **49**:1162 (1927).
15. L. G. Carpenter and L. G. Stoodley, *Philos. Mag*. **10**:249 (1930).
16. T. B. Douglas, A. F. Ball, and D. C. Ginnings, *J. Res. Nat. Bur. Stand*. **46**:334 (1951).
17. E. B. Amitin, E. G. Lebedeva, and I. E. Paukov, *Russ. J. Phys. Chem*. **53**:1528 (1979).
18. R. H. Busey and W. F. Giauque, *J. Am. Chem. Soc*. **75**:806 (1953).
19. M. V. Peralta-Martinez, Ph.D. Thesis (University of London, 2000).
20. G. Gehlhoff and F. Neumeier, *Verhandl. Deut. Physik. Ges*. **21**:201 (1919).
21. V. A. Vel'tishcheva, N. A. Kalakutskaya, and N. A. Nikol'skii, *Teploenergetika* **5**:80 (1958).
22. W. C. Hall, *Physica Rev*. **2**:1004 (1938).
23. W. C. Hall, Ph. D. Thesis (Univ. of Kansas, Lawrence, Kansas, 1936).
24. M. P. Prabhuram Saksena, *Ind. Eng. Chem. Fundam*. **21**:484 (1982).
25. G. Bush, H. J. Guntherodt, and P. Wyssmann, *Phys. Lett. A* **41**:29 (1972).